Global Journal of Computer Sciences: Theory and Research

Volume 12, Issue 1, (2022) 01-11 www.gjcs.eu

Mechanical design of a differential drive mobile robot platform

Suat Karakaya [1], Kocaeli University, Mechatronics Engineering Department, Kocaeli, Turkey

Suggested Citation:

Karakaya, S. (2022). Mechanical design of a differential drive mobile robot platform. *Global Journal of Computer Sciences: Theory and Research*. *12*(1), 01-11. https://doi.org/10.18844/gjcs.v12i1.6508

Received from December15, 2021; revised from February 15, 2022; accepted from April 01, 2022.
Selection and peer-review under responsibility of Assist. Prof. Dr. Ezgi Pelin Yıldız, Kafkas University,

Abstract

Mobile robotics science has been influenced by developments in electronics and software sciences and it has reached significant levels in the last 50 years. This study aims to present the design of an indoor mobile robot platform (MAVI-BOT). The platform consists of a chassis made of aluminum, a 2D light detection and ranging sensor (LIDAR), an inertial measurement unit (IMU), an infra-red camera and a LED projection, and an industrial PC. The platform, based on the differential drive model, has a 2-wheel drive. The active wheels are pneumatic and the third wheel is positioned as a rubber-filled caster. A study was also carried out to identify the actuators that met the given dynamic criteria. Real-time applications made on the developed wheeled mobile robot (WMR) are discussed.

Keywords: Actuator; LIDAR; MAVI-BOT; Mobile robot; mechanical design.

* ADDRESS FOR CORRESPONDENCE: Suat KARAKAYA* Mechatronics Engineering Department, Kocaeli University, Turkey.
E-mail address: suat.karakaya@kocaeli.edu.tr

1. Introduction

Mobile robotics science has been influenced by developments in electronics and software sciences and it has reached significant levels in the last 50 years. Today, mobile robotic technology is widely used in home environments, industrial environments, and outdoors. Technological developments have provided mobile robots with more flexibility and the ability to perform their tasks. Mobile robots can be controlled by operators or can be operated autonomously. Those with autonomic characteristics are usually called automated guided vehicles (AGV).

AGVs can improve the productivity and efficiency of industrial processes. However, it is not an easy task to design a safe, fully autonomous AGV system capable of evaluating all external factors. AGVs are mainly operated using electrical energy and are driven by electric motors [1]. It is a multidisciplinary field of study which includes proper electric motor and gears identification [2], mechanical body design, and electronic design stages.

In addition to the design of the control system, the feasibility of the sensors also plays an important role in AGV design. For this reason, the WMR illustrated in this study was designed not only with its electromechanical dimensions but also is supported by basic sensor groups. The mobile robots in literature are designed in various kinematics models such as omni-drive [3-4], differential [5-7] driving, skid-steering [8], and Ackerman-steering [9]. These models are preferred due to their load carrying capacities, maneuverability, and steering-control models. In this study, the differential-drive model is implemented in the WMR.

1.1. Literature review

1.1.1. Mechanical scheme

The kinematic design of the robot is based on the differential driving model. The mechanical design phase consists of the formation of a three-dimensional solid model of the base body, determination of the placement of actuators and other equipment on the robot, the manufacture of the chassis, and the selection of electric motors. The fasteners of the wheels are shown in detail. By calculating the weight distribution on the driven wheels, the total required torque is determined and these values are taken into consideration when selecting the appropriate electric motor.

1.1.1.1. Design of the Chassis

The chassis of the robot is made of 3 mm aluminum material. The front and back plates are bent with the bottom plate; the side plates are welded. The top cover is screwed on. There are two pneumatic wheels with 22 cm diameter and 6 cm thickness on the front side. There is a caster on the back of the robot as a balancer. A plastic handle is mounted on the backplate to facilitate the transport of the robot. LIDAR is fixed to the top cover with two custom-made metal plates. The solid model of the mobile robot platform is shown in Figure 1. On the backplane of the mobile robot platform, there are sockets for hardware inputs. The handle mounted on the same area acts as a transport tool and a mechanical buffer. On the inside of the robot frame, the DC motors are positioned along the wheel axis of rotation. The top cover can be mounted in two directions and the default direction of the robot can be flipped. The solid model and the exploded drawing of the fasteners required to connect the driven wheels to the chassis are shown in Figure 2. The active wheels are fixed by three screws between two opposing discs to assemble the motors to the robot chassis.

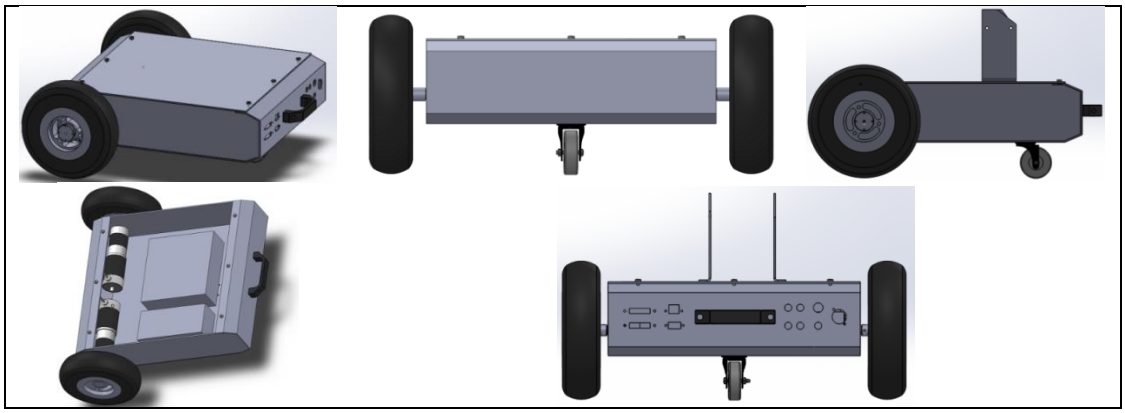

Fig 1. Solid model of the mobile robot platform

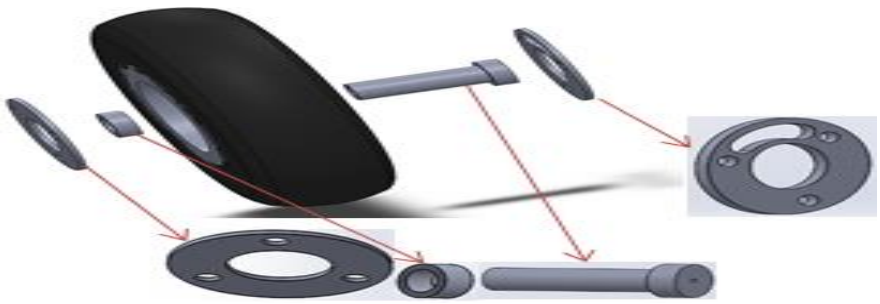

Fig 2. Exploded drawing of the wheel fasteners

It is aimed to prevent possible corrosion by passing bushings to the hub of the wheels which are fixed directly to the gear unit shaft. The LIDAR is mounted on the upper front of the robot by screwing it into the custom-made plates. LCD monitor and the camera-LED group are also located on the top cover. The robot has a plastic handle, a charging connector, an on-off switch, an on-off button for industrial computers, USB, Ethernet, and HDMI sockets, and 24V and 12V power connectors on the backplate. The LCD monitor connected to the built-in computer is mounted on the cover plate with a 45^{o} inclined attachment. The general appearance of the design as a result of manufacturing is given in Figure 3.

Fig 3. The general appearance of the manufactured WMR

1.1.1.2. Selection of the Appropriate Actuator

The required minimum and maximum torque requirements are calculated for the platform to satisfy the determined dynamic criteria. The evaluation was made not only in terms of torque requirement but also in weight and size. It is important that the weights on the active wheels are balanced and can provide friction-induced attachment. Several factors determine the distribution of the total weight of the robot chassis on wheels. These factors include the positioning of the wheels, the center of gravity of the chassis, the placement of the hardware on the chassis, and the positioning of the motors.

The dynamic requirements applied to the design of the mobile robot can be evaluated in a very wide framework. However, a design can be performed based on a set of determined parameters. The dynamic requirements identified as design criteria are given in Table 1. The parameters and symbols used in the force and torque equations are given in Table 2.

Table 1.

Design parameters of the WMR

Maximum linear velocity (V_{max}) = 1.5 m/s
Minimum time for reaching V_{max} (t_d) = 1 s
Weight of the WMR (W_r) = 25 kg-force
Weight on each drive wheel (W_{dw}) = 9.19 kg-force
Possible worst working surface (rolling friction coefficient for good concrete) (CRF = 0.01)
Maximum working slope (α) = 2°
Radius of the drive wheels (r_w) = 0.11 m

Firstly, force equations have been formed within the given criteria. The force components resulting from the rolling resistance (F_{all}), the working slope (F_{slope}), and inertial requirements (F_{acc}) were calculated separately. These components produce the total traction force.

Rolling resistance (F_{roll}) is the force required to push a vehicle onto a specific surface. The worst type of surface that the vehicle can face must be considered in the calculation of F_{roll}. The rolling resistance equation is given in (1).

$$F_{roll} = W_r \times c_{rf} = 25 \times 9.81 \times 0.01 = 2.45 \text{ N} \quad (1)$$

Slope resistance (F_{slope}) is the amount of force required to move a vehicle to a slope. The slope is considered to be the maximum possible working grade. The calculation of this component is given in (2).

$$F_{slope} = W_r \times \sin(\alpha) = 25 \times 9.81 \times \sin(2) = 8.55 \text{ N} \quad (2)$$

Inertial resistance (F_{acc}) is the force required to change from a steady state to a maximum speed within the desired time. The equation for F_{acc} is given in (3).

$$F_{acc} = \frac{m_r \times v_{max}}{t_d} = \frac{25 \times 1.5}{1} = 37.5 \text{ N} \quad (3)$$

The total traction force is calculated as the sum of these 3 calculated force components. The total tractional force equation is given in (4).

$$F_{total} = F_{roll} + F_{slope} + F_{acc} = 2.45 + 8.55 + 37.50 = 48.50 \text{ N} \quad (4)$$

To verify that the robot operates as intended for traction force and acceleration, the required wheel torque (T_{wr}) must be calculated depending on the traction effort. The total torque equation is given in (5).

$$T_{wr} = F_{total} \times r_w \times k_{rf} = 48.50 \times 0.11 \times 1.15 = 6.13 \text{ Nm} \quad (5)$$

Resistance factor refers to friction losses stemming from caster bearing and reduction gears. In practice, these type of losses affects the overall system by approximately between 10 and 15%.

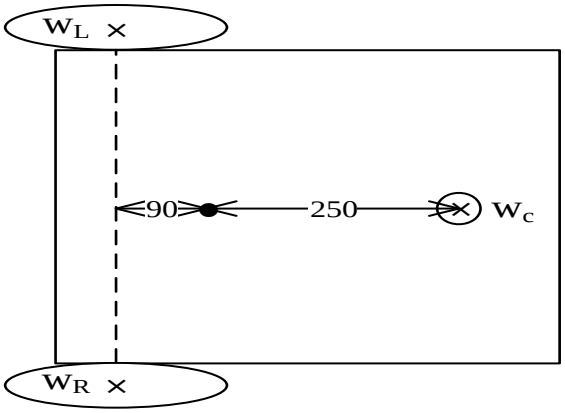

Fig 4. Free body diagram of the WMR: (dimensions are in millimetres)

After the required torque is calculated theoretically, the feasibility of this torque must be checked. It is desired that the wheels move without slipping. To calculate this critical torque value, the weight on each drive wheel must be known. This payload is calculated by basic equations given in (6), (7), (8), and (9) respectively. In the calculations, the free body diagram of the robot (given in Figure 4) has been utilized.

$$W_{dw} = W_R = W_L \quad (6)$$
$$2W_{dw} + W_c = W_r \quad (7)$$
$$18W_{dw} = 25W_c \quad (8)$$
$$W_r = 25 \rightarrow W_R = W_L = 9.18 \text{ kg-force} = 90.1 \text{ N (acceleration of gravity} = 9.81 \text{ m/s}^2) \quad (9)$$

The maximum allowed torque (non-slipping) on every single drive wheel is calculated by the equation (10).

$$T_{max} = W_{dw} \times c_{sf} \times r_w = 90.1 \times 0.6 \times 0.11 \sim= 5.95 \text{ Nm} \quad (10)$$

T_{max} represents the maximum amount of torque that can be applied before a slip occurs for each active wheel. T_{wr} for each active wheel (half of T_{wr}) must be less than T_{max} otherwise slipping will occur. Acceleration time – active wheel torque graph is given in Figure 5. This graph shows that the wheel

torque that provides the desired acceleration time is in the applicable torque zone. The best theoretical acceleration time that can be reached according to the given design criteria is ~0.45 seconds. If the amount of torque to each wheel exceeds 5.95 Nm, this power will not contribute to driving. As the torque values in the graph are the values per wheel, the total torque required to reach the desired maximum speed in 1 second is 3.068×2 ~= 6.13 Nm.

Table 2

Definitions of the abbreviations and the symbols

W_{dw}:	Weight on every single drive wheel [N]
W_L :	Weight on the left drive wheel [N]
W_R :	Weight on the right drive wheel [N]
W_c :	Weight on the caster [N]
W_r:	Weight of the WMR [N]
F_{total}:	Total force for traction [N]
F_{roll}:	Force emerged from rolling behavior [N]
F_{slope}:	Force emerged from maximum estimated slope [N]
F_{acc}:	Force emerged from desired acceleration [N]
c_{rf}:	Rolling friction coefficient (0.01 for good concrete)
c_{sf}:	Static friction coefficient (~0.6 for plastic on dry&clean concrete)
k_{rf}:	Resistance factor (~1.15)
r_w:	Radius of the drive wheels [m]
m_r:	Total mass of the WMR [kg]
V_{max}:	Maximum linear velocity [m/s]
α:	Maximum working slope [deg]
t_d:	Required time for reaching V_{max} [s]
T_{wr}:	Total wheel torque [Nm]
T_{max}:	Maximum allowed torque (non-slipping) on every single drive wheel [Nm]
●:	Center of gravity
×:	Payloads on wheels

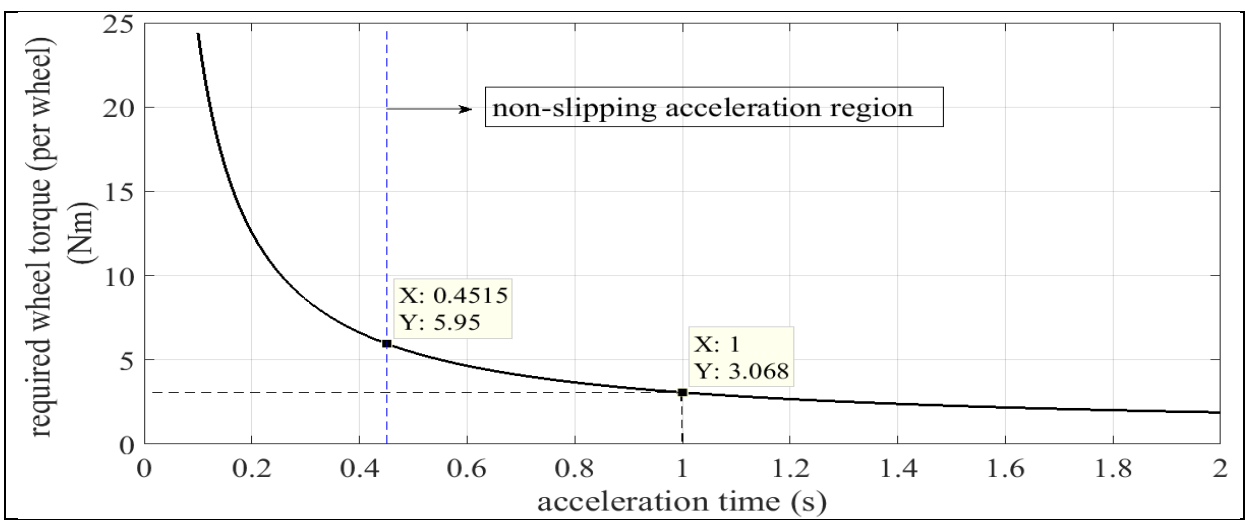

Fig 5. Acceleration time – active wheel torque graph

1.1.2. Hardware Scheme

The hardware components of the system can be listed as follows:

- Intel Core i7 3770 3,4 GHz IPC Mini-ITX NF9E-Q77- PC (Central PC)
- 7 inch LCD monitor
- Midwest Motion Products 158 rpm, 3.5 Nm 24 Volt gear motors and integrated 500 pulse encoders
- Pololu DC motor drive circuits
- Electronic control board
- SICK LMS100 LIDAR
- Remote control transceiver operating in 2.4 GHz radio frequency band
- Wireless modem
- USB Camera + LED projection

LIDAR, the central PC, camera, and led group that can be used in positioning applications, battery, regulator circuits, and motor drivers are the hardware components of the developed platform. There is also a control board for controlling the drivers and the remote control receiver. Developed in compliance with the STM32F4 card, this layer provides communication between the central PC and the electronic auxiliary equipment and speed control of the DC motors. Users can develop custom algorithms in the central PC and send the data package of calculated speed and direction information within a certain protocol to the control card via serial port. Instant motor speed and direction information can be read in the protocol format. With the remote controller, the speed of the robot can be controlled by reading the right-left, forward-back, and speed commands from three channels. The central PC can also be managed from a remote workstation via a wireless modem. LIDAR communicates via Ethernet port, camera hardware and LCD monitor communicates via USB connection. Power supplies of the hardware are provided with 12V and 24V regulator circuits. The power of the overall system is ensured by the Li-Po battery of 22.2V 16AH. The hardware diagram of the system is given in Figure 6.

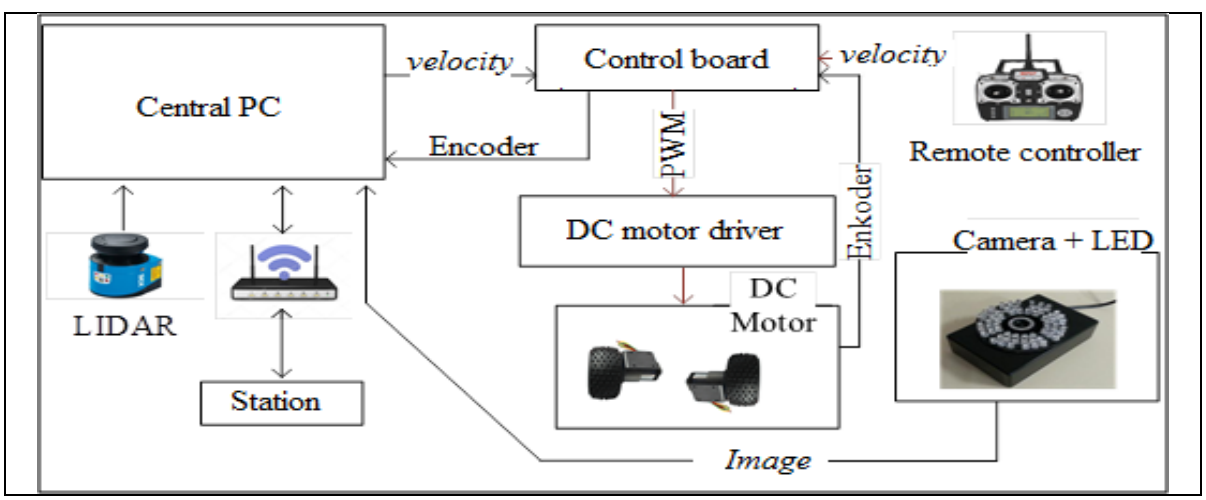

Fig 6. Hardware diagram

1.2. Purpose of study

Mobile robotics science has been influenced by developments in electronics and software sciences and it has reached significant levels in the last 50 years. This study aims to present a design of an indoor mobile robot platform (MAVI-BOT).

2. Materials and Methods

2.1. Data Collection

Experiments on basic topics in mobile robot science were performed by using the developed mobile robot platform. The approaches in the literature about indoor positioning systems and autonomous studies have been applied experimentally on the developed platform. The first experiment is based on the comparison of 3 localization approaches based on image processing techniques and estimation theory related to indoor positioning systems [10].

2.2. Participants

Corridor of Kocaeli University Faculty of Engineering Mechatronics Engineering Department was used as interior space.

3. Results

The equipment for the positioning system to be tested is installed in the ceiling section of the corridor space as depicted in Figure 7 and the 2D map of the indoor is processed as an image on the central PC. It has been observed that the WMR can be operated for 5 hours with the remote control without an external load.

Fig 7. Equipment for the positioning system mounted on the ceiling

During positioning tests, the mobile robot platform was moved in a random trajectory via a remote controller. The first exact position was measured before the robot started. The actual position was measured at 12 different points during the movement and the position errors that occurred at the points are logged as a table. Encoder-based odometer information, EKF-based position estimation (Source1), position information from the image processing-based system (Source2), and real position information from the point laser distance measuring instrument were recorded during the movement of the robot.

Table 3

Experimental results of the localization test

Real position (cm)		Source1 (cm)		Source2 (cm)		Error1 (cm)		Error2 (cm)	
x	y	x	y	x	y	x	y	x	y
762	360	759	356	767	354	-3	-4	5	-6
833	245	835	241	826	240	2	-4	-7	-5
930	174	932	175	937	179	2	1	7	5
1072	170	1075	167	1079	165	3	-3	7	-5
1176	232	1173	235	1172	237	-3	3	-4	5
1215	327	1216	331	1210	334	1	4	-5	7
1263	439	1265	440	1268	443	2	1	5	4
1353	500	1350	498	1357	496	-3	-2	4	-4
1495	433	1492	430	1490	429	-3	-3	-5	-4
1550	326	1554	322	1554	332	4	-4	6	4
1613	223	1617	219	1617	217	4	-4	4	-6
1678	86	1675	83	1685	91	-3	-3	7	6

The position data from the point laser distance measuring instrument was measured instantaneously by stopping the robot. These measurements are assumed to be the actual position information at the points where the robot is stopped and are considered as a reference for the other sources.

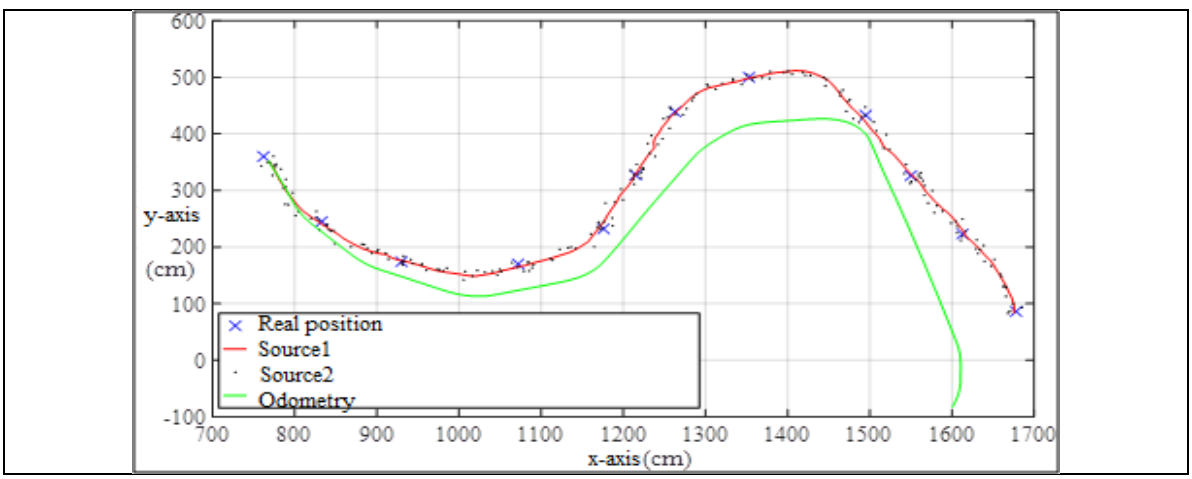

Fig 8. The trajectory of the WMR during the localization test

The trajectory of the WMR during the localization test is given in Figure 8. The actual positions and the localization measurements read from 3 sources are given in Table 3. During the experiments, autonomous path planning algorithms [11-13] were also studied. An example test environment is depicted in Figure 9. It is noted that while all equipment (PC, LIDAR, camera-projection group) is active under an extra 10 kg load, it can be operated in autonomous mode for approximately 2 hours. The path planning algorithms in the literature have been successfully applied to the robot in a course established with static obstacles.

Fig 9. Experimental environment of the autonomous task

4. Conclusion

As depicted, the equipment for testing the positioning system is installed in the ceiling section of the corridor and the indoor map is displayed on a central PC as an image. WMR can be controlled by remote control for five hours without any external load, according to experimental data. Also, Stopping the robot allowed the point laser distance measuring instrument to measure the position data immediately. The measurements at the points where the robot is stopped are assumed to represent the actual position and are used as a reference for the other sources.

Even though the PC, LIDAR, camera, and projection group can be operated autonomously under an extra 10 kg load, it can be used for approximately two hours. It has been demonstrated that path planning algorithms have been successful in planning paths for a robot traveling on a course with static obstacles in this study. The results of this study can be applied by practitioners in this field.

References

[1] Dudeja, H., Bagal, L., Zunjur, N., Jagadale, S. S., (2015). Mechanical Design of an Automated Guided Vehicle (AGV), International Journal of Research in Aeronautical And Mechanical Engineering, 3(5), 32-40.

[2] Lecture Notes of EML2322L, (2018). Department of Mechanical & Aerospace Engineering, University of Florida.

[3] Chu, B., Whee Sung, Y., (2013). Mechanical and Electrical Design about a Mecanum Wheeled Omni-Directional Mobile Robot, International Conference on Ubiquitous Robots and Ambient Intelligence (URAI), Jeju-South Korea.

[4] Chang, W., Youcef-Toumi, K., (1998). Modeling of an Omni-Directional High Precision Friction Drive Positioning Stage, IEEE International Conference on Robotics & Automation, Leuven-Belgium.

[5] Al-Sagban, M., Dhaouadi, R., (2012). Neural-Based Navigation of a Differential-Drive Mobile Robot, International Conference on Control, Automation, Robotics & Vision, Guangzhou-China.

[6] Wahab, M., Rios-Gutierrez, F., El Shahat, A., (2015). Energy Modeling of Differential Drive Robots, IEEE Southeast Conference, Florida-USA.

[7] Arvin, F., Samsudin, K., Nasseri, M. A., (2009). Design of a Differential-Drive Wheeled Robot Controller with Pulse-Width Modulation, Conference on Innovative Technologies in Intelligent Systems and Industrial Applications (CITISIA 2009), Sunway-Malaysia.

[8] Tang, S., Li, X., Zhang, Y., (2014). Effect of Body Rolling of Skid-Steering Wheeled Vehicle on Steering Characteristics, IEEE Conference and Expo Transportation Electrification Asia-Pacific (ITEC Asia-Pacific), Beijing-China.

[9] Kai, Y., Youjun, W., Zhongming, H., Xiaowen, Z., (2008). Optimum Design and Calculation of Ackerman Steering Trapezium, International Conference on Intelligent Computation Technology and Automation, Hunan-China.

[10] Karakaya, S., Ocak, H., Küçükyıldız, G., Kılınç, O., (2015). A Hybrid Indoor Localization System Based on Infra-red Imaging and Odometry, International Conference on Image Processing, Computer Vision & Pattern Recognition, Las Vegas-USA.

[11] Elizondo-Leal, J. C., Ramirez-Torres, G., (2010). An Exact Euclidean Distance Transform for Universal Path Planning, Electronics, Robotics, and Automotive Mechanics Conference, Cuernavaca-Mexico.

[12] Willms, A., Yang, S., (2008). Real-Time Robot Path Planning via a Distance Propagating Dynamic System with Obstacle Clearance, IEEE Transactions on System, Man and Cybernetics, 38(1), 884-893.

[13] Wan, T., Chen, H., Earnshaw, R., (2003). Real-Time Path Planning for Navigation in Unknown Environment, International Conference on Theory and Practice of Computer Graphics, Birmingham-UK.